

Enhancing Pt(IV) Complexes' Anticancer Activity upon Encapsulation in Stimuli-Responsive Nanocages

María Sancho-Albero,* Giorgio Facchetti, Nicolò Panini, Marina Meroni, Ezia Bello, Isabella Rimoldi, Massimo Zucchetti, Roberta Frapolli, and Luisa De Cola*

Platinum-based chemotherapy is the first-line treatment for different cancer types, and in particular, for malignant pleural mesothelioma patients (a tumor histotype with urgent medical needs). Herein, a strategy is presented to stabilize, transport, and intracellularly release a platinum^{IV} (Pt^{IV}) prodrug using a breakable nanocarrier. Its reduction, and therefore activation as an anticancer drug, is promoted by the presence of glutathione in neoplastic cells that also causes the destruction of the carrier. The nanocage presents a single internal cavity in which the hydrophobic complex (Pt(dach)Cl₂(OH)₂), (dach = *R,R*-diaminocyclohexane) is encapsulated. The *in vitro* uptake and the internalization kinetics in cancer model cells are evaluated and, using flow cytometry analysis, the successful release and activation of the Pt-based drug inside cancer cells are demonstrated. The *in vitro* findings are confirmed by the *in vivo* experiments on a mice model obtained by xenografting MPM487, a patient-derived malignant pleural mesothelioma. MPM487 confirms the well-known resistance of malignant pleural mesothelioma to cisplatin treatment while an interesting 50% reduction of tumor growth is observed when mice are treated with the Pt^{IV}, entrapped in the nanocages, at an equivalent dose of the platinum complex.

1. Introduction

Since cisplatin's discovery in 1965, organometallic molecules based on platinum have attracted huge attention in the biomedical field and it has been representing the gold standard in first-line chemotherapy for most cancers.^[1–4] Platinum-based drugs owe their anticancer activity to their unique ability to form covalent interactions with the nitrogen bases of the DNA, leading to secondary structures capable of stopping the transcription and replication of tumor cells.^[5] With the aim to discover different Pt-derived drugs with higher antitumoral efficacy and less systemic toxicity, in the last decades, the search for structural analogs of cisplatin has been encouraged leading to the development of second and third-generation of Pt-based drugs that entered the clinic (carboplatin, oxaliplatin or nedaplatin).^[6–8] Despite the improvements obtained, these complexes are still not selectively

accumulated in tumor cells, and toxic effects usually occur, forcing dose reductions or treatment delays that in turn reduce drug efficacy. Therefore, the complete cure of many cancer histotypes still represents a challenge. To overcome these problems, the introduction of structurally new ligands around the platinum center has been deeply studied.^[9–11] Also Pt^{IV} compounds have been employed^[12,13] as a prodrug that can, upon reduction to Pt^{II} become excellent therapeutic agents. This strategy has indeed shown an excellent reduction of the overall toxicity of the complex *in vivo* and activation in cancer cells triggered by the presence of the reducing biological molecule, glutathione, GSH. However, the often low solubility in water, the easy hydrolysis during circulation, and the difficulties to cross the cell membranes have attenuated the enthusiasm for such development.^[14,15]


An alternative approach to overcome these issues related to platinum chemotherapeutics relies on encapsulation in nanocarriers to deliver these molecules to target cancer tissues in the organisms.^[16] Some of the encapsulation strategies use nanotechnological products, such as inorganic particles, liposomes, and polymeric and co-polymeric nanoparticles (NPs), giving rise to a significant reduction in toxicity while incrementing their accumulation in cancer tissues compared with the naked drugs.^[17,18] Among them, silica NPs have demonstrated

M. Sancho-Albero, L. De Cola
Department of Biochemistry and Molecular Pharmacology
Istituto di Ricerche Farmacologiche Mario Negri IRCCS
Via Mario Negri 2, Milan 20156, Italy
E-mail: maria.sancho_albero@marionegri.it; luisa.decola@marionegri.it

G. Facchetti, I. Rimoldi, L. De Cola
Department of Pharmaceutical Science
DISFARM

Università degli Studi di Milano
Milan 20133, Italy

N. Panini, M. Meroni, E. Bello, M. Zucchetti, R. Frapolli
Laboratory of Cancer Pharmacology
Department of Oncology
Istituto di Ricerche Farmacologiche Mario Negri IRCCS
Via Mario Negri 2, Milan 20156, Italy

 The ORCID identification number(s) for the author(s) of this article can be found under <https://doi.org/10.1002/adhm.202202932>

© 2023 The Authors. Advanced Healthcare Materials published by Wiley-VCH GmbH. This is an open access article under the terms of the Creative Commons Attribution-NonCommercial-NoDerivs License, which permits use and distribution in any medium, provided the original work is properly cited, the use is non-commercial and no modifications or adaptations are made.

DOI: 10.1002/adhm.202202932

promising results in terms of Pt-containing molecules encapsulation and their release.^[19] In general, silica NPs, and in particular porous or capsules-like nanoparticles, have proven to improve the pharmacological properties of many anticancer drugs, such as their systemic toxicity and their poor water solubility, and present interesting advantages such as biocompatibility, degradability, large surface area for drug loading, stability, easy surface functionalization, and low cost.^[20,21]

The entrapping of platinum-based molecules has been achieved using different strategies, such as electrostatic interactions, taking advantage of the negatively charged silica and the often cationic nature of the complexes, or by functionalizing the NPs with different groups to covalently link the complexes. However, even with the best strategy, the loading yields are not higher than 10–20 wt% in most cases^[22–24] and rarely reach the tumor efficiently due to macrophage uptake or the size of the particles that prevent it to cross biological barriers.^[25] Recently, Wiesner et al.^[26–28] have published single pore silica materials that resemble a cage, possessing some apertures of a few nanometers and an internal cavity of about 7 nm. Modifying his synthetic strategy, we have recently reported organosilica nanocages (OSCs) that show several advantages compared with conventional mesoporous organosilica nanoparticles.^[29] These NPs are characterized by having a single inner pore of 8 nm and the ability to “break” on demand since the introduction of S–S moieties in the silica framework. Such disulfides are cleaved in the presence of reducing agents, such as GSH, which is one of the main mediators of cellular redox homeostasis and is highly overexpressed in cancer cells (1–10 mM).^[30,31] Therefore, the reduction of the disulfide to thiols leads to the destruction of the particles and consequently the cargo release. Moreover, these disulfide bonds provide the OSCs with a more hydrophobic behavior compared to non-breakable NPs and reduce the negative charge of the silica, thus helping hydrophobic molecules (such as neutral cisplatin derivatives) to be entrapped. In addition, the release of energetic highly ordered confined water molecules from the cavity has been demonstrated to be an entropic driving force in the encapsulation of non-water soluble molecules.^[32–34]

Such unusual morphology, the dual hydrophobic and hydrophilic behavior, and perhaps the specific chemistry of the disulfide are definitely responsible for what we discover: that these cage-like organosilica nanoparticles are not taken up by macrophages (even when they are functionalized with sugar ligands that favor cell phagocytosis)^[35] avoiding the immune system recognition.^[29] We have also demonstrated the encapsulation of out-of-equilibrium luminescent platinum complex aggregates and their delivery in cell cytoplasm with the evolution, upon carrier destruction, toward thermodynamic stable fibers formation.^[36]

Starting from the above considerations and promising results, herein, we present the preparation of breakable cage-like organosilica particles (ssOSCs) characterized by a biodegradable framework and an internal single cavity in which a hydrophobic Pt^{IV} complex 5, (Pt(dach)Cl₂(OH)₂), acting as a prodrug therapeutic has been encapsulated.

Since platinum compounds are the backbone of the first-line chemotherapy against malignant pleural mesothelioma, a rare and aggressive tumor histotype with an urgent medical need, we decided to test our approach on this type of cancer. Indeed,

despite the addition of the anti-folate pemetrexed and more recently of the antiangiogenic bevacizumab, the prognosis still remains poor for malignant mesothelioma patients. For this reason, our data were finally corroborated both in vitro and in vivo in MPM487 malignant mesothelioma patient-derived xenograft, with biphasic morphology. We evaluated the uptake and the internalization kinetics in cancer cells by confocal microscopy and a deeper analysis of the therapeutic properties of the Pt-loaded NPs, by flow cytometry, demonstrated the successful release of the complex, the reduction of the toxic Pt^{II} drug inside the cells and the cell death.

2. Results and Discussion

2.1. Characterization of Prodrug Pt(dach)Cl₂(OH)₂

Platinum complexes containing chiral diaminocyclohexane (dach) as a chelating ligand have gained increasing attention after Oxaliplatin (FDA-approval in 2002) for their ability to overcome the cross-resistance with cisplatin. The hydrophobic nature and the bulkiness of the dach ligand along with its intrinsic chirality make the corresponding metal complexes endowed with a different pharmacological profile in comparison to cisplatin, due to a different interaction with DNA polymerases and the ability to elude mismatch repair proteins and damage recognition machinery.^[37–39]

Pt^{IV}(dach) complexes are particularly intriguing in this field considering their major stability toward deactivating nucleophiles and the possibility to be rapidly reduced by endogenous molecules to the corresponding Pt^{II} active form once in the cell. Starting from these premises, Pt(dach)Cl₂(OH)₂ complex was synthesized according to Figure S1, Supporting Information. Pt(dach)Cl₂ 4 was prepared according to Dhara's method^[40] as the intermediate K₂PtI₄ is much more reactive toward (dach) substitution thus affording the product in higher yield and purity. The subsequent reaction with AgNO₃ led to the formation of Pt(dach)(H₂O)₂(NO₃)₂ which was converted to the Pt(dach)Cl₂ upon treatment with a saturated NaCl aqueous solution. The oxidation step to the Pt^{IV} complex Pt(dach)Cl₂(OH)₂ 5 was finally realized in the presence of 30% w/w of H₂O₂ in water and confirmed by the different spectroscopic analyses (Figure S1, Supporting Information).

2.2. Pt Complex Encapsulation in ssOSCs

The nanoparticles used for the encapsulation of the metal complexes, as already mentioned, are similar to the beautiful “silicages” previously reported by Wiesner and co-workers,^[26–28] however, we have covalently linked disulfide groups as part of the silica framework. The easy reduction of the disulfide to thiols with a consequent breaking of the S–S bond allows to destroy the nanocages inside cancer cells, due to the presence of GSH, resulting in the cargo release. Luminescent Pt^{II} complexes have been entrapped within silica cage-like particles in a previously published work by our group.^[29,36] After the loading of Pt^{IV} molecules into the particle's cavity, they were washed by dispersion-centrifugation cycles to remove any physisorbed Pt molecule on the surface.

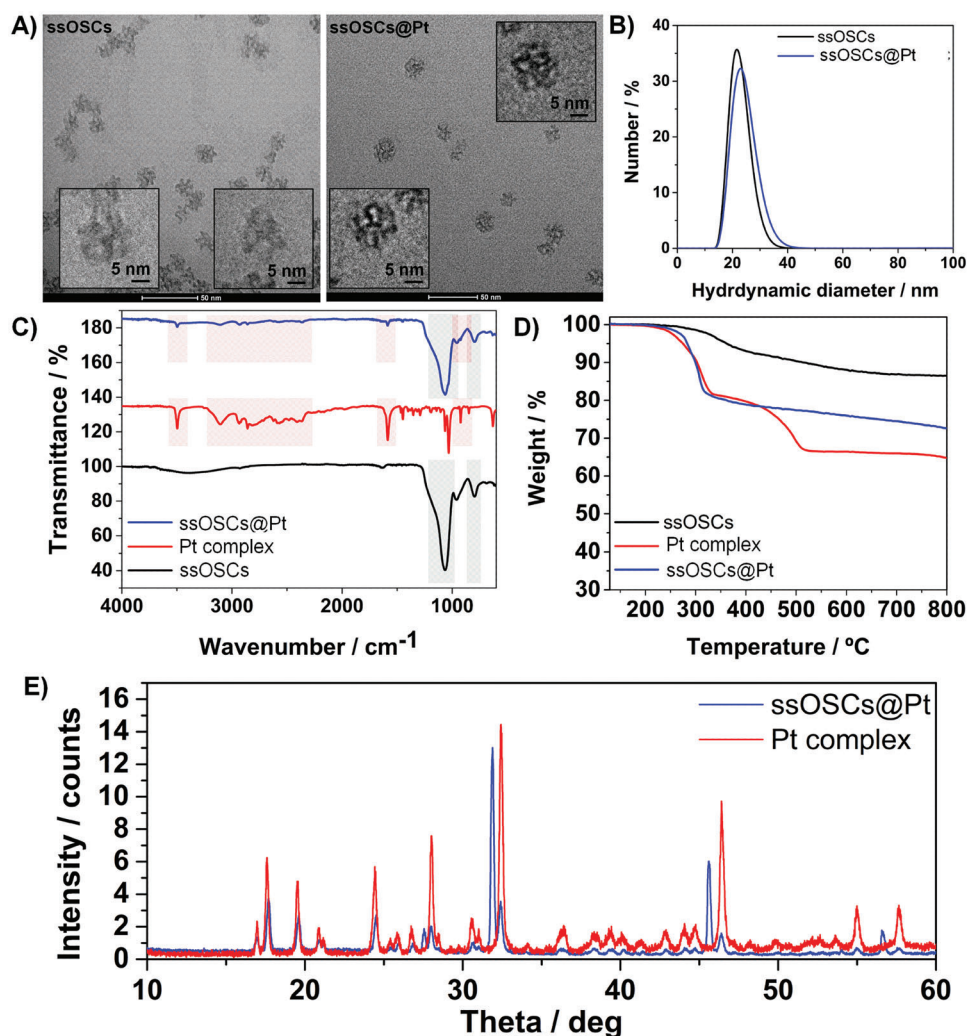


Figure 1. Characterization of ssOSCs and ssOSCs@Pt. A) TEM images of ssOSCs and ssOSCs@Pt. The insets show the TEM images of single OSCs. B) Hydrodynamic diameter of empty and loaded ssOSCs in water obtained by DLS. C) FTIR transmission spectra recorded on ssOSCs, Pt complex, and Pt-loaded ssOSCs. D) TGA analysis of the nanoparticles and the Pt complex. E) XRD analysis of the Pt^{IV} and ssOSCs@Pt.

Transmission electron microscopy (TEM) images revealed a cage-like morphology with a size of about 18 nm and an internal single cavity of 8 nm (Figure 1A). When Pt(dach)Cl₂(OH)₂ 5 was encapsulated, the nanoparticles were significantly more electron-dense and in the images, a significantly darker contrast is observed compared to empty ssOSCs. Dynamic light scattering (DLS) measurements of the empty and loaded NPs were in agreement with TEM images, exhibiting a hydrodynamic diameter of ≈20 nm (Figure 1B). The surface charge of the ssOSCs and the ssOSCs@Pt were -15.2 ± 1.09 and -14.09 ± 2.29 mV, respectively. These data confirmed that no residual cationic surfactant was present in the empty ssOSCs particles after the synthesis and purification of the NPs. FT-IR spectra (Figure 1C) revealed the presence of the disulfide bond incorporated within the silica framework of the nanoparticles. The characteristic absorption bands of the methyl groups connected to the disulfide unit occur at 1456 and 1354 cm⁻¹ attributed to the -CH₂ wagging and deformation vibration. All the peaks coming from the Pt^{IV} complex were clearly observed in the ssOSCs@Pt, confirming again

the encapsulation of the compound in the cage-like particles. The amount of disulfide bonds and the loading of Pt^{IV} encapsulated were assessed by thermogravimetric assay (TGA), indicating the presence of the disulfide linker to be ≈15%.

High-angle annular dark-field scanning transmission electron microscopy (HAADF-STEM) and energy dispersive X-ray spectroscopy (EDX) were employed to determine the presence of the Pt in the internal cavity of the ssOSCs, as well the disulfide (S-S) groups in the silica framework. As it is shown in Figure S2, Supporting Information, it was possible to observe: 1) the presence of the Platinum encapsulated in the NPs; 2) the signal of the sulfur coming from the disulfide bonds present in the silica framework; and 3) the Silicon present as the silica constituting the particles.

To determine the encapsulation loading, thermogravimetric analysis and microwave plasma atomic emission spectroscopy (MP-AES) analysis were performed. TGA analysis allowed estimating the loading of the Pt compounds being ≈20 wt% upon comparison with the thermogram recorded for the empty ssOSCs (Figure 1D). For quantifying the exact amount of

Pt(dach)Cl₂(OH)₂ 5 encapsulated, MP-AES revealed 0.12 +/- 0.01 mg of atomic Pt/mg of ssOSCs, thus a 12% of loading, being in good agreement with TGA analysis (as in TGA a small contribution of retained dH₂O could be contributed to the weight decrease obtained).

Finally, to confirm the presence of the Pt(dach)Cl₂(OH)₂ 5 inside the nanoparticles' pore, an XRD analysis was carried out. Figure S3, Supporting Information, shows how the ssOSCs were amorphous (no distinct peaks were observed). On the contrary, when analyzing the ssOSCs@Pt, the crystalline structure of the Pt compound could be also observed (compared with the non-encapsulated molecule) demonstrating that it was successfully entrapped into the NPs (Figure 1E). Indeed, the shift of the peaks are indicating that the complexes are inside the cavity.

2.3. In Vitro Internalization Experiments

Motivated by the possibility of using this ssOSCs@Pt for cancer treatment, the breakability of the NPs and their potential therapeutic effect were probed in vitro to demonstrate that the release and activation of the anticancer drug can take place in a complex medium such as living cells. As a well-established in vitro cancer cell model, HeLa cells were used to test the antitumoral activity of the Pt-loaded ssOSCs. In order to have a homogeneous size distribution of the purified ssOSCs@Pt, nanoparticle suspension was extensively sonicated (15 min) before being used.

The internalization of ssOSCs@Pt in HeLa cells was first evaluated by confocal microscopy and then quantified by flow cytometry. For internalization experiments, ssOSCs@Pt were labeled with the sulfo-Cy5-NHS, a red-emitting dye, as described in the Experimental Section. Cy5-labeled NPs exhibited a characteristic maximum emission peak at 670 nm when they were excited at 633 nm (Figure S4, Supporting Information). In Figure 2 and Figures S5 and S6, Supporting Information, cells were permeabilized and stained with Hoechst 33 342 to label the nuclei (blue) and with phalloidin-Alexa568 to stain the cytoskeletal actin fibers (green). Z-stack orthogonal projections were carried out in order to demonstrate the presence of the nanoparticles inside the cytosol. Figure 2A shows the results of HeLa cells incubated with 15 μg mL⁻¹ of ssOSCs@Pt. Nanoparticles were clearly internalized forming aggregates inside the cell cytoplasm, probably inside vesicles following the endosomal route as it is reported in the literature.^[41] The fluorescence of the nanoparticles was clearly and significantly incremented after 24 and 48 h of incubation. Confocal images of the uptake of ssOSCs@Pt in HeLa cells, incubated with 10 and 5 μg mL⁻¹, are included in the Supporting Information (Figures S5 and S6, Supporting Information). Internalization dynamics of the nanoparticles in HeLa cells were also evaluated using flow cytometry. As demonstrated by confocal microscopy and flow cytometry after 4 h of incubation, some NPs were already observed inside cells. However, the presence of the ssOSCs@Pt inside the cytoplasm of the cells increased significantly after 24 h of incubation, reaching a maximum at 72 h (Figure 2B). This trend was clearly observed for all the tested doses, demonstrating a concentration-dependent internalization. Cy5 fluorescence histogram plots of the analyzed cells at the different time points incubated with ssOSCs@Pt (5, 10, and 15 μg mL⁻¹) are included in Figure S7, Supporting Information.

Taking into account the poor solubility of complex 5 in water, it is expected that ssOSCs@Pt are taken up by cells following an endocytic translocation. Then, because of the presence of the disulfide bonds in the silica structure, the presence in the cytosol of cancer cells of GSH in a concentration higher than 5 mM was able to trigger the breakability of the disulfide-containing organosilica leading to the release of the active reduced Pt^{II} complex.

2.4. In Vitro Uptake of Pt-Loaded ssOSCs

To determine the internalization and the efficacy of the ssOSCs@Pt as antiproliferative agents, the loaded nanoparticles were studied using HeLa cells and the MPM487 human malignant mesothelioma cells (see next sections). In HeLa cells, the particles were incubated for different times: 3, 6, 24, and 48 h and using different concentrations of NPs (0.5 to 30 μg mL⁻¹). Empty nanoparticles (ssOSCs) were used as a control. Figure 3A shows that for the lowest time-point (3 h) only the highest doses (30 and 15 μg mL⁻¹) caused a significant decrease in cell viability. On the contrary, for the highest time point (48 h), a significant decrease in cell viability was observed even for the lower doses. According to Figure 3A, the antiproliferative effects of ssOSCs@Pt were accompanied by a change in the cell morphology visible after 48 h of incubation. Cells exhibited irregular shapes with a large number of vesicles and apoptotic bodies within them. For the control, empty ssOSCs, no cytotoxic effects were observed at any of the doses and time points tested.

Tumor cells were then incubated with ssOSCs@Pt (10, 5, and 2.5 μg mL⁻¹) for 24 and 48 h and the percentage of live and dead cells was determined by flow cytometry (Figure 3B and Figures S8 and S9, Supporting Information). In agreement with the metabolic cell viability assay, empty ssOSCs exhibited no cytotoxic effects and the percentage of live and dead cells was comparable to the control cell cultured (nontreated) at both time points. On the contrary, in the case of ssOSCs@Pt, a significant increase in dead cells was observed. In particular, dead cells showed a 50% of increase after their incubation with 10 μg mL⁻¹ Pt^{IV}-loaded silica-cage particles during 24 and 48 h.

To evaluate the mechanism of action of the ssOSC@Pt, exponentially growing HeLa cells were incubated with 5, 10, and 15 μg mL⁻¹ of NPs, and the cell cycle perturbation was evaluated at 48 h after treatment. Cell cycle data are depicted in Figure 4. A significant decrease in the percentage of cells in the G1 phase and consequently, an accumulation of cells in the S and G2M phases of the cycle compared with the control (untreated cells), were clearly observed after treatment with Pt^{IV}-loaded ssOSCs. On the contrary, no significant differences were found in the percentage of cells in phases G1, G2/M, and S when cells were incubated with empty ssOSCs. In particular, when HeLa cells were incubated with 5 μg mL⁻¹ of ssOSCs@Pt, 47.7% of the cells were in phase G1 compared to 74.54% of the non-treated cells (negative control). Upon increasing the concentration of ssOSCs@Pt to 10 and 15 μg mL⁻¹, the percentage of cells in phase G1 decreased even more, up to 34.98% and 12.45%, respectively. As expected, the Pt^{IV} compound internalized by the cells through the nanoparticles, induced an S and G2/M block. On the contrary, empty NPs did not show any effect on cell distribution in cell cycle phases. This result confirmed the nanoparticle uptake

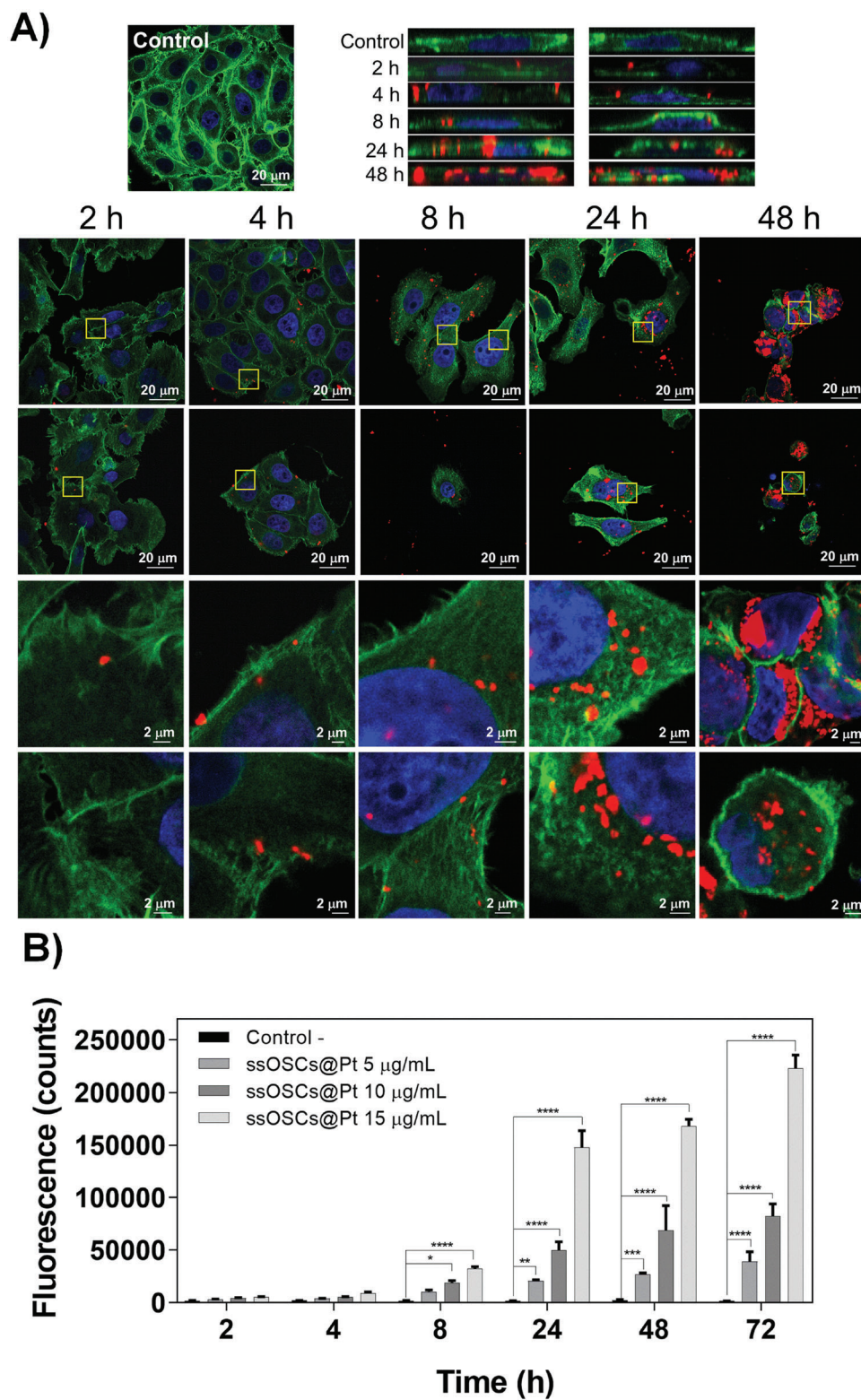


Figure 2. ssOSC@Pt internalization in HeLa cells. A) Confocal Z-stacks of cells incubated with the Pt-loaded silica-cage particles ($15 \mu\text{g mL}^{-1}$) during 2, 4, 8, 24, and 48 h. The insets and the orthogonal projections show that red-labeled nanoparticles are surrounded by green actin fibers. B) Flow cytometry-based kinetics of the internalization process presented as mean fluorescence counts. The internalization of the nanoparticles is clearly concentration and time-dependent.

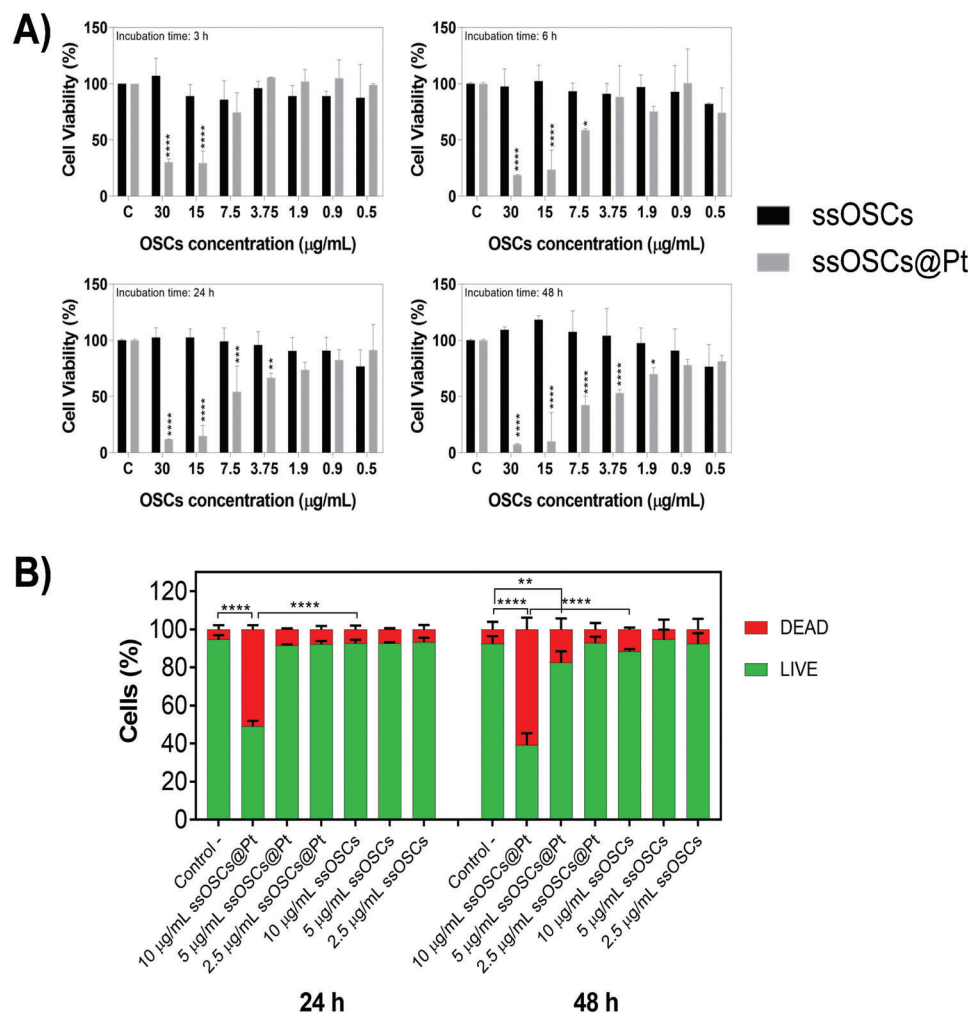


Figure 3. Cell viability experiments. A) MTT assay results for ssOSCs and ssOSCs@Pt in HeLa cells. B) Flow cytometry analysis of live/dead cells after their incubation with both empty and Pt-loaded ssOSCs.

capacity previously demonstrated by flow cytometry (Figure 2B), showing a dose and time-dependent behavior. More interestingly, these results suggest the capability of the nanoparticles to release the compound after the cells' uptake and internalization and the activation of the Pt^{IV} to an active Pt^{II} species leading to cancer cell death.

2.5. Colocalization Studies of ssOSCs in MPM487 Human Malignant Mesothelioma Cells

For studying the internalization and trafficking of the ssOSCs within the cancer target cells, MPM487 cells were incubated with the NPs for 2, 4, 8, 24, and 48 h. During these time points, the colocalization of the NPs in the different compartments was assessed by confocal microscopy. To this end, early endosomes were labeled with a specific EEA1 antibody, the cell nuclei with Hoechst, the lysosomes with LysoTracker, and the ssOSCs with Cy5. When evaluating early endosomes (Figure 5A), confocal microscopy images revealed high yellow fluorescence pixels on the MPM487 cells cytoplasm, that is, the merging of the green and

red fluorescence, which corresponds with the early endosomes and the ssOSCs. On the contrary, after 24 and 48 h, most of the degraded silica NPs were located in the lysosomal organelles for being eliminated by the cells, evidencing that the NPs have been already broken and their inner cargo has been released to the cytosol of the cells.

2.6. Intracellular Activation of Pt(dach)Cl₂(OH)₂ Prodrug in MPM487 Human Malignant Mesothelioma Cells

In order to understand the role of the nanocages in the protection and intracellular release of the drug, we have compared the growth inhibitory effect induced by cisplatin, DPP (positive control), ssOSCs@Pt, the prodrug 5, and the active compound 4, in different doses. We have employed MPM487 malignant pleural mesothelioma. After 6 h of incubation, the excess drugs or nanomaterials, have been removed by washing twice with PBS and adding fresh cell culture media. Different incubation times have been observed by metabolic assays (see Figure 6). As can be seen, after 24 h, neither the DPP, Pt^{IV}, and Pt^{II} molecules

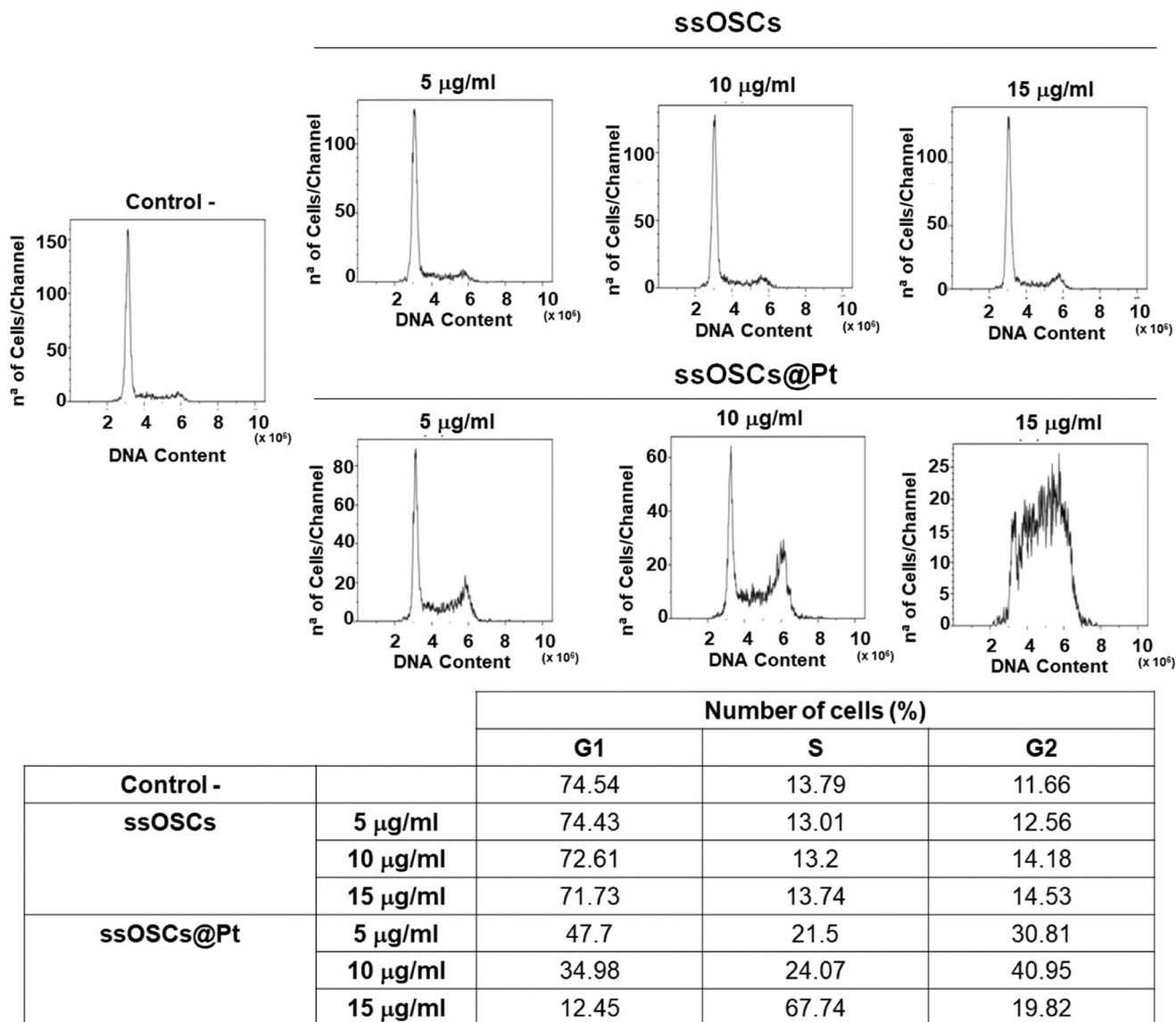


Figure 4. Cell cycle analysis. Cell cycle evaluation of HeLa cells incubated with ssOSCs and ssOSCs@Pt (15, 10, and 5 µg mL⁻¹) during 48 h.

induced a strong inhibition of cell growth (Figure 6B). On the contrary, ssOSCs@Pt exhibited cell viability decreased at the highest doses. After 48 h, cells treated with ssOSCs@Pt and with the active drug 4 exhibited a similar antitumoral efficacy, although the nanoparticles were more effective compared with the naked active drug, Figure 6C. The MPM487 human malignant mesothelioma cells treated with the highest doses of Pt^{IV} (5) exhibit lower cell viability caused by the intracellular activation of the prodrug. After 72 h, higher cell mortality has been observed, as expected, but a similar trend is observed for all the analyzed compounds. Interestingly, the graph shows that with a very low concentration of the Pt drug encapsulated in the nanocages, the effect is even better than the Pt^{II} drug alone. In addition, the comparison with prodrug 5, demonstrates the lower activity of the Pt^{IV} system. As a control experiment, the empty ssOSCs did not cause any toxicity on cells at any of the time-point and concentrations tested.

In summary, these data evidenced the breakability of the loaded ssOSCs triggered by the reduction of the disulfide-containing organosilica and demonstrated the release and reduction of 5 to 4 leading to an intracellular activation of the drug inside the cancer cells (Figure 6A). We believe that the nanocages prevent the degradation and sequestration of the drug before reaching the tumoural cells and for the efficacy of the ssOSCs@Pt is already visible at a concentration as low as 2.5 µM. These results, together with the analysis of the DNA content shown in Figure 4 demonstrated that the Pt compound is able to interact with the target cells by exerting cytotoxic effects through its binding to the DNA of cancer cells. Previously, it has been demonstrated that exposure to Pt-based DNA damaging agents induced cell arrest by activating cell cycle checkpoint thanks to its interaction with the DNA.^[42] Our results are in concordance with previous literature and envisaged DNA damage caused by the Pt compound leading to cell death.^[43]

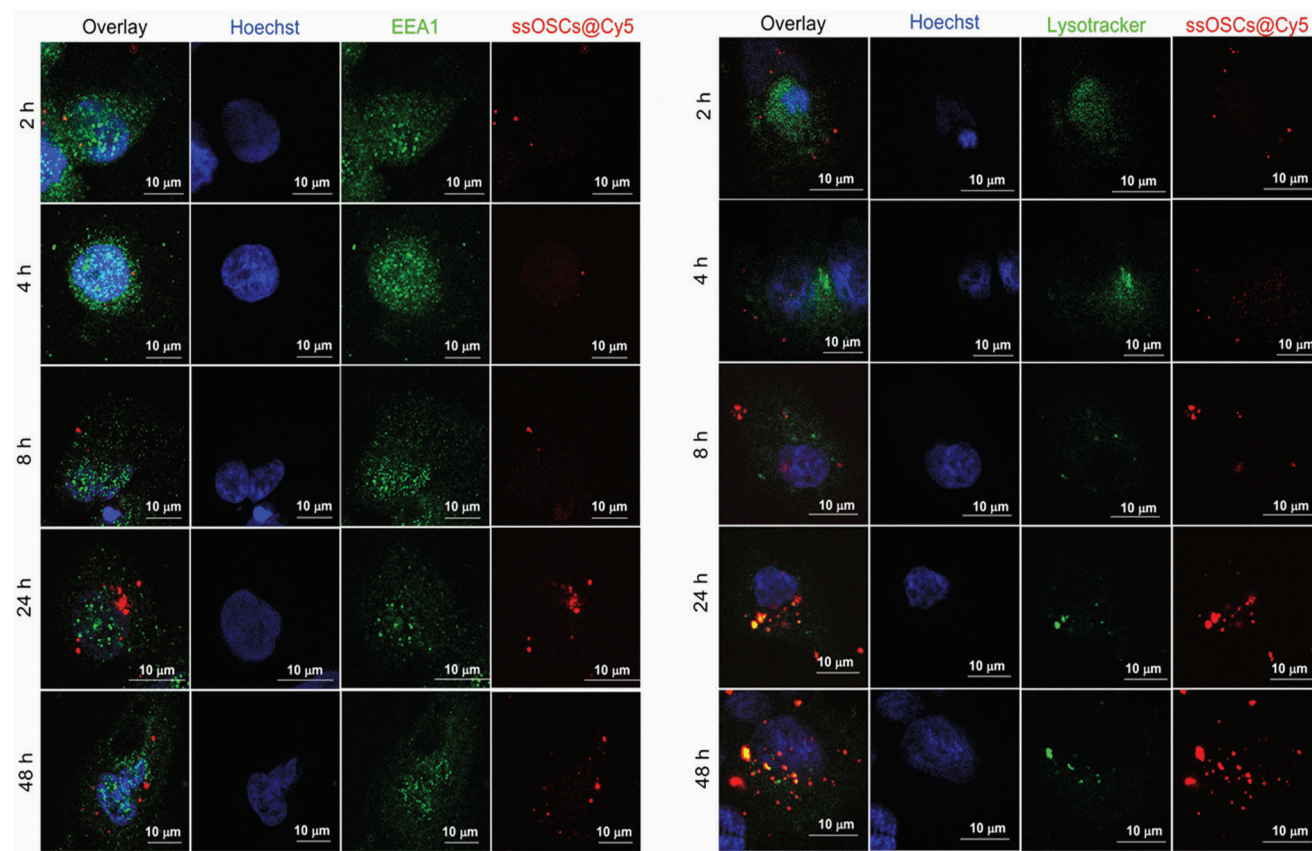


Figure 5. Colocalization study in MPM487 cells. Confocal images of MPM487 human malignant mesothelioma cells incubated with ssOSCs@Cy5 for 2, 4, 8, 24, and 48 h. A) The green channel corresponds to early endosomes labeled with anti-EEA1 antibody, the blue channel shows the nuclei stained with Hoechst, and the red channel shows the ssOSCs functionalized with Cy5. B) Lysosomes were labeled in green with Lysotracker and nuclei and ssOSCs were stained with Hoechst and Cy5, respectively.

2.7. In Vivo Therapeutic Effect of ssOSCs@Pt in a Mesothelioma Model

To evaluate the in vivo therapeutic potential of the new vector herein designed, the MPM487 malignant pleural mesothelioma PDX model with a biphasic morphology was used in mice. The tumor was engrafted subcutaneously and grown until tumor weight reached $\approx 200\text{--}250$ mg. The therapeutic effect of the ssOSCs@Pt was compared with cisplatin (DPP) as it is the platinum-approved drug established as the gold standard in the first-line chemotherapy of mesothelioma cancer and the encapsulated drug is not water-soluble. DPP was administered intravenously, twice a week, at a dose of 2.5 mg kg^{-1} . Pt-loaded ssOSCs were given at the equivalent Pt content, with the same schedule. Control mice received an intravenous injection of saline solutions. Tumor growth was monitored, over a period of 37 days. The antitumor efficacy was expressed as T/C% where T and C are the mean tumor weight of treated and control mice, respectively. For more details, see the Experimental Section. This tumor model is poorly sensitive to the main clinically used drugs, with only gemcitabine treatment able to cause a slight but significant reduction in tumor growth.^[44]

As shown in **Figure 7**, while DDP is completely ineffective, ssOSCs@Pt treatment caused a significant tumor growth de-

lay ($p < 0.05$) resulting in a T/C of 54.6% on day 26. With both treatments, a body weight loss (BWL) always $<10\%$ was observed suggesting a good tolerability profile of the new nanoformulation. Previous data obtained in our mesothelioma models highlights impressive differences between the good cytotoxic effect observed in vitro and the scant tumor response observed in vivo.^[44] These differences may be explained by the in vivo presence of the tumor microenvironment. It may play a dual role: 1) decreasing cancer cell susceptibility to anticancer drugs via the expression of various factors such as chemokines and cytokines, and 2) impeding efficient drug intratumor distribution. Our data demonstrate that the last issue can be addressed by the use of tumor-specific nanocarriers such as ssOSCs@Pt.

3. Conclusion

We have demonstrated the use of OSCs as suitable nanocarriers to host, stabilize, and release Pt^{IV} complexes as a prodrug that can be activated intracellularly to the very toxic Pt^{II} analog, while the same reduction causes the destruction of the carriers. The data show that the antitumoral activity is present for all the drugs in vitro but only for the ssOSCs@Pt in vivo. In a detailed analysis of the mesothelioma cells, metabolic cell viability and flow cytometry demonstrated that the internalization of ssOSCs@Pt

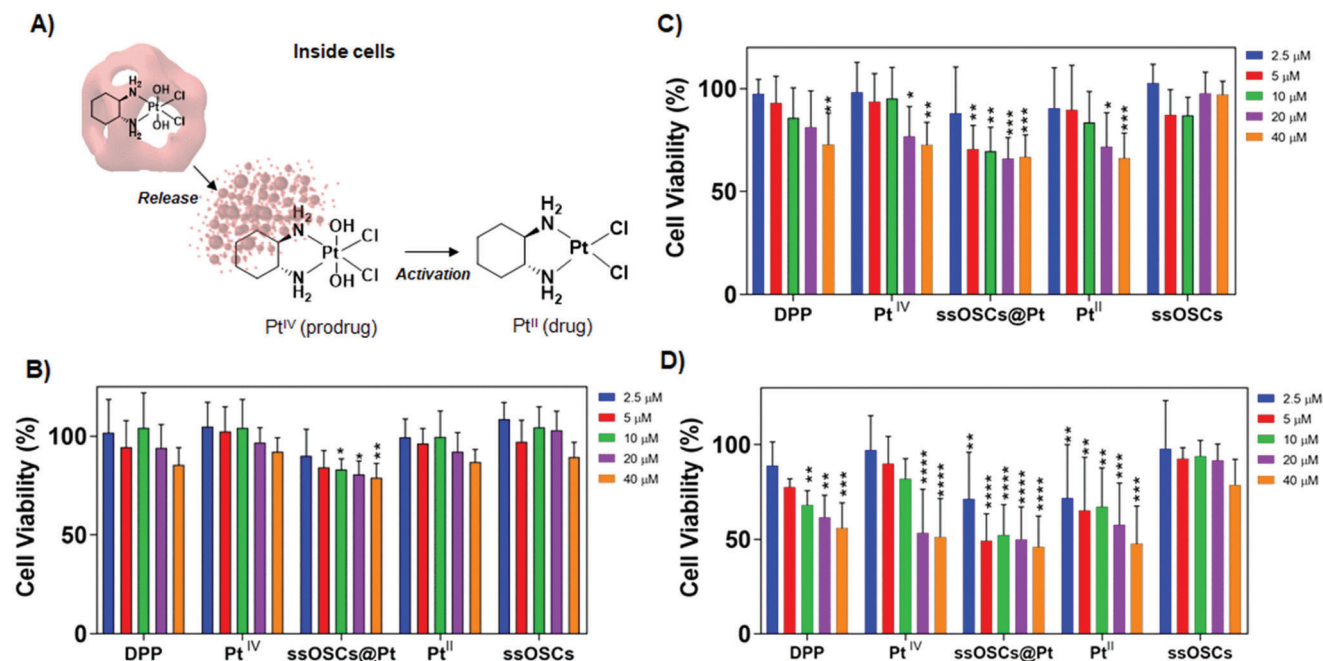


Figure 6. Growth inhibition with anticancer Pt-based agents and activation of Pt^{IV} prodrug in MPM487 human malignant mesothelioma cells. A) Schematic representation of the degradation of the ssOSCs@Pt followed by the release of the Pt^{IV} prodrug and its conversion to the active drug (Pt^{II}) inside the cells. B–D) Viability of cells after incubation with the different Pt compounds during 6 h and drug washing out for 24, 48, and 72 h, respectively. Each point is the mean of five replicates; bars represent the standard deviation. Asterisks indicate a significant difference in the mean of cell viability against control.

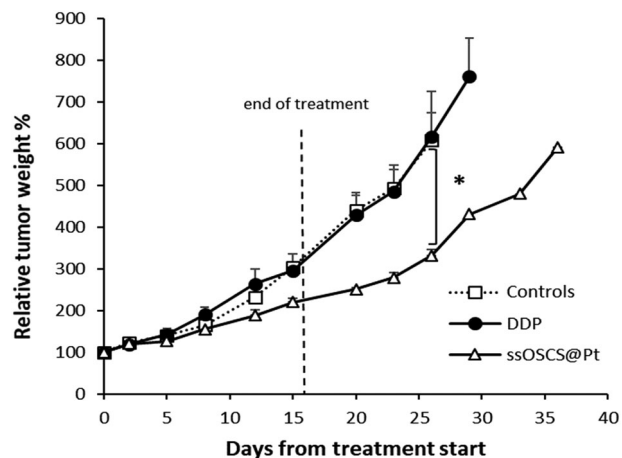


Figure 7. Antitumor activity study. Mice bearing MPM487 human malignant mesothelioma xenograft were treated with ssOSCs@Pt or DDP at the dose of 2.5 mg kg⁻¹ (DDP equivalent) twice a week for 3 weeks. * $p < 0.05$ (Mixed model ANOVA).

and the release of the active Pt^{II} molecules produced a decrease in tumor cell viability even at very low concentrations. The antitumoral properties of the Pt-loaded cage-like nanoparticles were finally demonstrated in hard-to-treat cancer such as mesothelioma. The treatment with the reference compound, DPP, the ssOSCs@Pt, and the vehicle (saline) resulted in a significant reduction in tumor growth only when the animals were treated with the ssOSCs@Pt. For the first time, in this work, we prove the efficacy of the nanocages as non-toxic nanocarriers, their ability to

release on demand the drug inside cancer cells, and more importantly, their efficacy in a platinum-resistant xenograft model of malignant mesothelioma.

4. Experimental Section

Materials: All the materials were acquired from Merck and used as received. Sulfo-cy5-NHS ester was purchased from Lumiprobe. Phalloidin-Alexa-568 and Hoechst 33 342 were purchased from Life Technologies.

Synthesis of Pt Complex Pt(dach)Cl₂(OH)₂: Platinum complex 5 Pt(dach)Cl₂(OH)₂ (dach = R,R-diaminocyclohexane) was synthesized starting from K₂PtCl₄ using Dhara's method (Scheme S1, Supporting Information).^[40] K₂PtCl₄ (2 g, 0.005 mol) was dissolved in 50 mL of degassed water and a solution of KI (2.8 g, 0.017 mol, 3.5 equiv.) in 10 mL of water was added under a nitrogen atmosphere. The reaction mixture immediately turned brown. After having stirred the solution for a further 45 min, R,R-diaminocyclohexane (dach) (550.3 mg, 1 equiv.) in 10 mL of water was added dropwise affording Pt(dach)I₂ 3 as a yellow precipitate. The mixture was stirred overnight in the dark under a nitrogen atmosphere and the precipitate Pt(dach)I₂ was then filtered and washed extensively with water and acetone (2.54 g, 0.0045 mol, 94% yield). Pt(dach)I₂ was then suspended in 50 mL of water and AgNO₃ (1.53 g, 2 equiv.) was added to the slurry and the resulting mixture was stirred for 24 h at room temperature. The AgI precipitate was then removed by filtration and the product Pt(dach)Cl₂ 4 was obtained as a yellow solid by adding dropwise a saturated NaCl solution. The product Pt(dach)Cl₂ was washed extensively with water, acetone, and ethanol (1.68 g, 0.0044 mol, 98% yield). The synthesis of Pt(dach)Cl₂(OH)₂ 5 was carried out according to the procedure reported in the literature.^[40] Pt(dach)Cl₂ (1.68 g, 0.0044 mol) was suspended in 50 mL of water and 15 mL of H₂O₂ 30% w/w was added. The slurry was heated at 50 °C overnight in the dark. The obtained precipitate was filtered off and washed with water and acetone and product 5 was isolated as a pale-yellow solid (1.28 g, 0.003 mol, 68% yield).

All manipulations involving air-sensitive materials were carried out in an inert atmosphere glove box or using standard Schlenk line techniques, under an atmosphere of nitrogen or argon in oven-dried glassware. All solvents were used as anhydrous. $^1\text{H-NMR}$ and $^{13}\text{C-NMR}$ spectra were recorded on a Bruker DRX Avance 300 MHz equipped with a non-reverse probe (BBI). MS analyses were performed by using a Thermo Finnigan (MA, USA) LCQ Advantage system MS spectrometer with an electrospray ionization source and an "Ion Trap" mass analyzer. The MS spectra were obtained by direct infusion of a sample solution in MeOH under ionization, ESI positive. Elemental analyses were performed using a Perkin Elmer SeriesII/CHNS/O 2400 Analyzer. FTIR spectra were collected by using a Perkin Elmer (MA, USA) FTIR Spectrometer "Spectrum One" in a spectral region between 4000 and 450 cm^{-1} and analyzed using the transmittance technique with 32 scans per ion and 4 cm^{-1} resolution.

Breakable Organosilica Nanocages Synthesis: ssOSCs were synthesized following a previously published protocol.^[26,29] Briefly, cetyltrimethylammonium bromide (CTAB) (408 mg, 1.12 mmol) was dissolved in 50 mL of deionized water at 50 °C in a 100 mL round-bottom flask. The solution was stirred for 30 min at 250 rpm with a magnetic stirrer (Teflon, cylindrical geometry, 1 cm length). Then, aqueous NH_3 (12.5 μL , 28% in water) was added and the stirring speed was increased to 750 rpm. Subsequently, a mixture of tetraethyl orthosilicate (TEOS) (448.1 μL , 2 mmol) and bis[3-(triethoxysilyl)propyl]disulfide (BTDS) (102.8 μL , 0.223 mmol) were added and the mixture was stirred at 750 rpm, during 20 h at 50 °C.

The ssOSCs dispersion was purified by dialysis against $\text{EtOH}/\text{H}_2\text{O}/\text{AcOH}$ (1/1/0.007 v/v/v) mixture during 72 h, then against $\text{EtOH}/\text{H}_2\text{O}$ (1/1 v/v) for 24 h and finally against dH_2O during 24 h. The dialysis solutions were replaced every 12 h.

The resulting ssOSCs were characterized by TEM using a T20-FEI microscope with a LaB6 electron source fitted with a "SuperTwin" objective lens allowing a point-to-point resolution of 2.4 Å. For TEM observations, samples were pipetted onto a TEM copper grid. The size distribution and the surface charge of the nanoparticles were obtained by employing a DLS instrument. The DLS measurements were performed on dispersions of ssOSCs in dH_2O (pH 7) using a Zetasizer Ultra equipment equipped with Multi-Angle Dynamic Light Scattering (MALDLS) technology from Malvern Panalytical and using the software ZS Xplorer. Fourier transform infrared (FTIR) spectra were recorded using a Shimadzu IRAffinity-1 spectrometer. The transmittance spectrum was collected using a spectral resolution of 1 cm^{-1} accumulating 64 scans from 600 to 4000 cm^{-1} .

TGA was conducted on a Netzsch model STA 449 fi Jupiter instrument. The samples (0.5–3 mg) were kept at 100 °C for 30 min for stabilization, then heated from 130 to 800 °C at a speed of 10 °C min^{-1} , before being held at this temperature for a further 30 min at the end of the measurement. The analysis was carried out under a 20 mL min^{-1} airflow.

The HAADF-STEM imaging at 300 kV and the elemental analysis of the ssOSCs@Pt were carried out by EDX, with an Analytical Titan (FEI company) high-resolution transmission electron microscope with a spherical aberration corrector.

For internalization experiments, nanoparticles were labeled with sulfo-Cy5-NHS probe. First, a sulfo-Cy5-silane was prepared. To do that, a solution of sulfo-Cy5-NHS ester (0.5 mg, 0.643 μmol) was suspended in dry dimethylsulfoxide (DMSO). Then, APTES (4.5 μL , 0.142 M in dry DMSO) was added and the reaction mixture was allowed to stir for 30 min in the dark. The reaction mixture was used for post-synthesis and post-Pt-encapsulation grafting of the ssOSCs without further purification. Emission spectra of Cy5 functionalized NPs were recorded on a Horiba Jobin-Yvon IBH FL-322 Fluorolog 3 spectrometer equipped with a 450 W xenon arc lamp, double grating excitation, and emission monochromators (2.1 nm mm^{-1} of dispersion; 1200 grooves per mm) and a TBX-04 single photon-counting detector. The samples were excited by a wave laser at $\lambda_{\text{ex}} = 633 \text{ nm}$. The emission of the samples was collected in the range from 640 to 820 nm.

Pt(dach) $\text{Cl}_2(\text{OH})_2$ 5 Loading into ssOSCs: Pt(dach) $\text{Cl}_2(\text{OH})_2$ 5 encapsulation into the particles was achieved using a slightly modified procedure.^[36] 50 mg of NPs were suspended in 10 mL of EtOH. In parallel, Pt compound (50 mg) was also dissolved in 10 mL of EtOH. Both solu-

tions were sonicated for 10 min separately. After that, they were mixed and briefly sonicated for a further 20 min and stirred for 12 h at room temperature. Subsequently, to recover Pt-loaded ssOSCs (ssOSCs@Pt), they were washed with EtOH (10 mL \times 3) and water (10 mL \times 3). The resulting material was resuspended in PBS and was kept at 4 °C for the in vitro and in vivo experiments. Some of the material was lyophilized for characterization. The content of the Pt compound loaded inside the ssOSCs was quantified by MP-AES, using a quadrupole mass spectrometer (4100 MP-AES, Agilent Technologies, USA). NPs were digested with 10% Aqua regia ($\text{HNO}_3 + 3\text{HCl}$) in dH_2O . Calibrations were carried out using Pt standards in 20 regia water ranging from 0 to 15 ppm. FT-IR spectra were also carried out as previously mentioned to corroborate the presence of the Pt complex within the nanoparticles. Furthermore, TGA allowed determining the loading upon comparison with the thermogram recorded for the empty ssOSCs. Finally, TEM analysis was performed.

In Vitro Internalization Experiments: HeLa cells were grown in Dulbecco's modified Eagle's medium (DMEM, Biowest, France) supplemented with 10% fetal bovine serum (FBS, GIBCO, USA), 1% penicillin/streptomycin (Biowest, France), and maintained at 37 °C in a 3.5% CO_2 -humidified atmosphere under normoxic conditions. The internalization of ssOSCs@Pt was evaluated by confocal microscopy and by flow cytometry. First, the cellular uptake was determined by confocal microscopy (Nikon A1 confocal scan unit with a 100 \times 1.49 NA oil immersion objective managed by NIS elements software). Cells were seeded at a density of 3 \times 10⁴ cells onto 20 mm coverslips (in a 24-well plate) and cultured for 24 h. In order to visualize the Pt-loaded ssOSCs, they were labeled with sulfo-Cy5-NHS as previously described.^[29] Then, Cy5-labeled ssOSCs@Pt (5, 10, and 15 $\mu\text{g mL}^{-1}$) were resuspended in DMEM and were added to the cells during 2, 4, 8, 24, and 48 h. Afterward, cells were fixed with paraformaldehyde (PFA) 4% and finally washed three times with PBS. In order to label the cytoplasm actin, cells were stained with phalloidin-Alexa568 (Invitrogen, USA). Hoechst 33 342 was used to observe the nuclei. The cells' capability to internalize the ssOSCs@Pt was evaluated in exponentially growing cells. Briefly, 5 \times 10⁴ cells were seeded onto a 6-well plate. Then, they were treated with Pt-loaded and Cy5-labeled ssOSCs@Pt at the concentration of 5, 10, and 15 $\mu\text{g mL}^{-1}$. At specific time points (2, 4, 8, 24, 48, and 72 h after the treatment), cells were collected and analyzed by flow cytometry using Cytoflex LX instrument (Beckman coulter), and the data were analyzed by Kaluza Software (Beckman Coulter). Non-treated cells were used to set the gate and both the percentage of positive cells and the mean fluorescence intensity were taken into account to assess nanoparticle internalization. For the detection of Cy5-labeled ssOSCs@Pt, an excitation wavelength of 633 nm was used. The emitted signal was collected with BP 610/10 filters. All the samples were analyzed acquiring at least 10000 events.

In Vitro Antitumoral Activity of ssOSCs@Pt: To determine the antiproliferative properties of Pt-loaded ssOSCs, the MTT Cell Viability assay (ThermoFisher Scientific) was employed following manufacturer instructions. During the evaluation, HeLa cells were seeded into a 96-well plate at a concentration of 4 \times 10³ cells per well in 100 μL of the above-mentioned medium. After incubation at 37 °C for 24 h, the medium was changed to 100 μL of freshly prepared medium enriched with ssOSCs@Pt or with ssOSCs (5, 10, 20, 50, and 100 $\mu\text{g mL}^{-1}$), and cells were cultured for another 3, 6, 24, and 48 h. At these different time points, cells were washed with PBS and then treated MTT test. Briefly, tetrazolium solution (20 μL of 5 mg mL^{-1}) was added to each well and incubated for 4 h. The medium was replaced with acidified isopropanol (0.04 M HCl) to dissolve the purple precipitate and the absorbance intensity was measured at 570 nm using a plate reader (Infinite M200, Tecan). Data were expressed as percentages of controls (non-treated cells) for three separate replicates. The percentage of dead cells after the treatment of ssOSCs@Pt was also estimated by flow cytometry comparing the differently treated samples with control (non-treated) cells at different time points. As previously described, exponentially growing cells were seeded onto a 6-well plate and incubated with the empty and Pt-loaded ssOSCs, respectively (2.5, 5, and 10 $\mu\text{g mL}^{-1}$) for 24 and 48 h. After these two time points, both detached cells and cells present in the supernatant were stained with 2.5 $\mu\text{g mL}^{-1}$ of Propidium iodide (ProboKine, Heidelberg, Germany). The percentage of live and dead

cells was determined by acquiring at least 10 000 events with a CytoFlex LX Flow Cytometer (Beckman Coulter). Cells without Propidium Iodide were used as the negative control.

Finally, the cell cycle was analyzed by flow cytometry via DNA staining. As previously mentioned, exponentially growing cells were seeded onto a 6-well plate and incubated with the NPs (with or without Pt complex) (5, 10, and 15 $\mu\text{g mL}^{-1}$) for 48 h. After trypsinizing the cells, they were washed with PBS and fixed in 70% ethanol. Finally, $1-2 \times 10^6$ cells were incubated overnight with 1 mL of 25 $\mu\text{g mL}^{-1}$ Propidium Iodide (ProboKine, Heidelberg, Germany) plus 12.5 μL of 1 mg mL^{-1} RNase (Merck, Darmstadt, Germany) PBS. All the samples were analyzed acquiring at least 10 000 events with a CytoFlex LX Flow Cytometer (Beckman Coulter).

Colocalization Studies of ssOSCs in MPM487 Human Malignant Mesothelioma Cells: The presence of the ssOSCs in MPM487 cells and their colocalization were evaluated by confocal microscopy. Cells were seeded at a density of 2×10^4 onto 20 mm coverslips (in a 24-well plate) and incubated with ssOSCs labeled with Cy5 (15 $\mu\text{g mL}^{-1}$) during 2, 4, 8, 24, and 48 h. For labeling the early endosomes, cells were fixed with PFA 4% (20 min) and immunocytochemistry was performed. Samples were blocked with PBS/BSA 1% and permeabilized with Tryton-100X. Then, anti-EEA1 (1/500, rabbit mAb, Abcam ab109110) was incubated with the cells for 1 h and finally, the secondary antibody anti-rabbit IgG Alexa Fluor 488 (1/400 Invitrogen) was incubated for one more hour. Lysosomes were labeled with LysoTracker Green DND-26 (Life Technologies) by incubating the molecule with the cells for 45 min at a concentration of 65 μM . Nuclei were stained with Hoechst and the ssOSCs were functionalized with Cy5 as previously mentioned. Cells were observed under confocal microscopy as described before.

Intracellular Activation of Pt(dach)Cl₂(OH)₂ Prodrug: MPM487 human malignant mesothelioma cells were cultured with Ham's F-10 (Sigma Aldrich) supplemented with 10% FBS (GIBCO, USA), 1% penicillin/streptomycin (Biowest, France), and L-glutamine and incubated at 37 °C with 5% CO₂.

For evaluating the activation of the P^{IV} prodrug encapsulated within the ssOSCs, MPM487 human malignant mesothelioma cells were seeded in a 96-well plate format (2000 cells per well) and incubated for 24 h before treatment. Each well was then replaced with fresh media containing DPP (40–2.5 μM), ssOSCs, ssOSCs@Pt (40–2.5 μM), Pt(dach)Cl₂(OH)₂ (40–2.5 μM), and Pt(dach)Cl₂ (40–2.5 μM). Non-treated cells were considered as the negative control. The amount of ssOSCs@Pt added was considered at the equivalent Pt content. After 6 h of incubation, cells were washed three times with PBS and treated with fresh media for an additional 24, 48, and 72 h. Cell viability was determined by MTT as described above. All conditions were normalized to the untreated cells (100%). Experiments were performed in triplicates.

In Vivo Efficacy of ssOSCs@Pt in a Mesothelioma Model: 7-week-old female athymic nude mice were obtained from Envigo. Animals were housed and handled under specific pathogen-free conditions in the Institute's Animal Care Facilities, which meet international standards. They were regularly checked by a certified veterinarian who is responsible for health monitoring, animal welfare supervision, experimental protocols, and procedure revision.

The following laws, rules, and guidelines governing the use and care of laboratory animals were followed during procedures involving animals: Italian governing law (D.lgs. 26/2014; Ministry of Health authorization n.19/2008-A given on March 6, 2008); Guidelines for the welfare and use of animals in cancer research (Workman P. BJC (2010) 102,1555-1577), the NIH Guide for the Care and Use of Laboratory Animals (2011 edition), and EU directives and guidelines (EEC Council Directive 2010/63/UE). They are all in accordance with Mario Negri Institutional Regulations and Policies that provide internal authorization for persons conducting animal experiments (Quality Management System Certificate – UNI EN ISO 9001:2008 – Reg. No. 6121. MPM487 human malignant mesothelioma xenograft was obtained from cells isolated from pleural effusion of a patient with stage III biphasic pleural mesothelioma as previously described.^[43] Mice were engrafted subcutaneously with 3 × 3 mm tumor fragments. The increasing tumor masses were measured using a Vernier caliper, and the tumor weight (1 mm³ = 1 mg) was estimated using the for-

mula: length × (width)²/2. Mice were randomly assigned to the treatment group (four mice per group) after tumor weight reached ≈200–250 mg.

Cisplatin (DDP) was administered intravenously, twice a week, at a dose of 2.5 mg kg^{-1} . Pt-loaded ssOSCs were given at the equivalent Pt content, with the same schedule. Control mice received an intravenous injection of saline. Tumor growth was monitored, twice a week, up to 1500–2000 mg (ethical end-point). The antitumor efficacy was expressed as T/C% where T and C are the mean tumor weight of treated and control mice, respectively. Tolerability was evaluated based on BWL, clinical observation, and mortality.

Statistics: All the data are indicated as mean ± SD. Statistical analysis of the in vitro data and the significant differences among the means were analyzed by two-way analysis of variance (ANOVA) for multiple comparisons by Dunnett's multiple comparisons test (GraphPad Software). Statistically significant differences were expressed as follows: * $p < 0.05$; ** $p < 0.01$; *** $p < 0.0001$; **** $p < 0.00001$. In vivo experiments were analyzed using a mixed model ANOVA.

Supporting Information

Supporting Information is available from the Wiley Online Library or from the author.

Acknowledgements

R.F. and L.C. contributed equally to this work. This project received funding from the European Union's Horizon 2020 research and innovation program under grant agreement No 964386 project acronym "MimicKEY". M.S.-A. thanks to the financial support from Mario Negri Young Investigator Grant (project number 8702) and the AIRC- Foundation for cancer research for a Postdoctoral fellowship in Italy (26907-2021). The authors kindly thank Dr. Victor Sebastian for the electronic microscopy images performed in the LMA and the ICMA from the University of Zaragoza. The authors also thank Dr. Nuria Navascués for the MP-AES carried out in the ICMA from the University of Zaragoza.

Open access funding provided by BIBLIOSAN.

Conflict of Interest

The authors declare no conflict of interest.

Data Availability Statement

The data that support the findings of this study are available from the corresponding author upon reasonable request.

Keywords

mesothelioma, nanocages, organosilica, platinum complexes, tumor reduction

Received: November 14, 2022
Revised: January 27, 2023
Published online: March 28, 2023

- [1] B. Rosenberg, L. Van Camp, T. Krigas, *Nature* **1965**, 205, 698.
- [2] I. Kostova, *Recent Pat. Anti-Cancer Drug Discovery* **2006**, 1, 1.
- [3] I. E. L. Stephens, A. S. Bondarenko, U. Grønberg, J. Rossmesl, I. Chorkendorff, *Energy Environ. Sci.* **2012**, 5, 6744.

- [4] T. Mironava, M. Simon, M. H. Rafailovich, B. Rigas, *Toxicol. In Vitro* **2013**, *27*, 882.
- [5] T. Makovec, *Radiol. Oncol.* **2019**, *53*, 148.
- [6] I. Ali, W. A. Wani, K. S. Haque, *Anti-Cancer Agents Med. Chem.* **2013**, *13*, 296.
- [7] V. Pekarik, J. Gumulec, M. Masarik, R. K. Adam, *Curr. Med. Chem.* **2013**, *20*, 534.
- [8] J. Hrabeta, V. Adam, T. Eckschlager, E. Frei, M. Stiborova, R. Kizek, *Anti-Cancer Agents Med. Chem.* **2016**, *16*, 686.
- [9] F. Sacco, M. Tarchi, G. Ferraro, A. Merlino, G. Facchetti, I. Rimoldi, L. Messori, L. Massai, *Int. J. Mol. Sci.* **2021**, *22*, 10551.
- [10] V. Coccè, I. Rimoldi, G. Facchetti, E. Ciusani, G. Alessandri, L. Signorini, F. Sisto, A. Gianni, F. Paino, A. Pessina, *Pharmaceutics* **2021**, *13*, 2101.
- [11] G. Facchetti, N. Ferri, M. G. Lupo, L. Giorgio, I. Rimoldi, *Eur. J. Inorg. Chem.* **2019**, *2019*, 3389.
- [12] A. Annunziata, A. Amoresano, M. E. Cucciolito, R. Esposito, G. Ferraro, L. Iacobucci, P. Imbimbo, R. Lucignano, M. Melchiorre, M. Monti, C. Scognamiglio, A. Tuzi, D. M. Monti, A. Merlino, F. Ruffo, *Inorg. Chem.* **2020**, *59*, 4002.
- [13] X. Li, Y. Liu, H. Tian, *Bioinorg. Chem. Appl.* **2018**, *2018*, 8276139.
- [14] M. Imran, W. Ayub, I. S. Butler, Z. Rehman, *Coord. Chem. Rev.* **2018**, *376*, 405.
- [15] A. Lastner, I. Poetsh, J. Mayr, J. V. Burda, A. Roller, P. Heffeter, B. K. Keppler, C. R. Kowol, *Angew. Chem., Int. Ed.* **2019**, *58*, 7464.
- [16] Z. Tao, B. Toms, J. Goodisman, T. Asefa, *ACS Nano* **2010**, *4*, 789.
- [17] T. Boulikas, *Oncol. Rep.* **2004**, *12*, 3.
- [18] J. De Toro, L. Herschlik, C. Waldner, C. Mongini, *Oncol. Rep.* **2014**, *12*, 3.
- [19] M. Varache, I. Bezeverkhyy, G. Weber, L. Saviot, R. Chassagnon, F. Baras, F. Bouyer, *Langmuir* **2019**, *35*, 8984.
- [20] B. Pelaz, C. Alexiou, R. A. Alvarez-Puebla, F. Alves, A. M. Andrews, S. Ashraf, L. P. Balogh, L. Ballerini, A. Bestetti, C. Brendel, S. Bosi, M. Carril, W. C. W. Chan, C. Chen, X. Chen, X. Chen, Z. Cheng, D. Cui, J. Du, C. Dullin, A. Escudero, N. Feliu, M. Gao, M. George, Y. Gogotsi, A. Grünweller, Z. Gu, N. J. Halas, N. Hampp, R. K. Hartmann, et al., *ACS Nano* **2017**, *11*, 2313.
- [21] J. Shi, P. W. Kantoff, R. Wooster, O. C. Farokhzad, *Nat. Rev. Cancer* **2017**, *17*, 20.
- [22] M. M. Khan, A. MAdni, N. Tahir, F. Parveen, S. Khan, N. Jan, A. Ali, M. Abdurrahim, U. Farooq, M. I. Khan, *Int. J. Nanomed.* **2020**, *15*, 2207.
- [23] D. B. Wright, M. T. Proetto, M. A. Touve, N. C. Gianneschi, *Polym. Chem.* **2019**, *10*, 2996.
- [24] F. Chen, F. Zhang, Y. Wang, J. Peng, L. Cao, Q. Mai, M. Ge, L. Li, M. Chen, W.-F. Dong, Z. Chang, *Front. Bioeng. Biotechnol.* **2022**, *10*, 860949.
- [25] J. Jia, Z. Wang, T. Yue, G. Su, C. Teng, B. Yan, *Chem. Res. Toxicol.* **2020**, *33*, 1055.
- [26] T. Aubert, J.-Y. Huang, K. Ma, T. Hanrath, U. Wiesner, *Nat. Commun.* **2020**, *11*, 4695.
- [27] K. Ma, Y. Gong, T. Aubert, M. Z. Turker, T. Kao, P. C. Doershuk, U. Wiesner, *Nature* **2018**, *558*, 577.
- [28] K. Ma, H. Sai, U. Wiesner, *J. Am. Chem. Soc.* **2012**, *134*, 13180.
- [29] L. Talamini, P. Picchetti, L. M. Ferrerira, G. Sitia, L. Russo, M. B. Violatto, L. Travaglini, J. F. Alarcon, L. Righelli, P. Bigini, L. De Cola, *ACS Nano* **2021**, *15*, 9701.
- [30] J. Bonet-Aleta, M. Sancho-Albero, J. Calzada-Funes, S. Irusta, P. Martín-Duque, J. L. Hueso, J. Santamaria, *J. Colloid Interface Sci.* **2022**, *617*, 704.
- [31] H. J. Forman, H. Zhang, A. Rinna, *Mol. Aspects Med.* **2009**, *30*, 1.
- [32] B. Baumgartner, J. Hayden, J. Loizillon, S. Steinbacher, D. Grosso, B. Lendl, *Langmuir* **2019**, *35*, 11986.
- [33] F. Biedermann, V. D. Uzunova, O. A. Scherman, W. M. Nau, A. De Simone, *J. Am. Chem. Soc.* **2012**, *134*, 15318.
- [34] F. Biedermann, W. M. Nau, H.-J. Schneider, *Angew. Chem., Int. Ed.* **2014**, *53*, 11158.
- [35] T. Mosaiab, D. C. Farr, M. J. Kiefel, T. A. Houston, *Adv. Drug Delivery Rev.* **2019**, *151–152*, 94.
- [36] P. Picchetti, G. Moreno-Alcántar, L. Talamini, A. Mourgout, A. Aliprandi, L. De Cola, *J. Am. Chem. Soc.* **2021**, *143*, 7681.
- [37] F. Arnesano, A. Pannunzio, M. Coluccia, G. Natile, *Coord. Chem. Rev.* **2015**, *284*, 286.
- [38] Z. Xu, Z. Wang, Z. Deng, G. Shu, *Coord. Chem. Rev.* **2021**, *442*, 213991.
- [39] F. Piccinelli, C. NArdon, M. Bettinelli, A. Melchior, M. Tolazzi, F. Zinna, L. Di Bari, *ChemPhotoChem* **2022**, *6*, 202100143.
- [40] S. R. A. Khan, S. Huang, S. Shamsuddin, S. Inutsuka, K. H. Whitmire, Z. H. Siddik, A. R. Khokhar, *Bioorg. Med. Chem.* **2000**, *8*, 515.
- [41] M. Sancho-Albero, N. Navascués, G. Mendoza, V. Sebastián, M. Arrebo, P. Martín-Duque, J. Santamaria, *J. Nanobiotechnol.* **2019**, *17*, 16.
- [42] V. J. Menon, E. J. Peterson, K. Valerie, N. P. Farrell, L. F. Povirk, *Biochem. Pharmacol.* **2013**, *86*, 1708.
- [43] D. Salerno, G. L. Beretta, G. Zanchetta, S. Brioschi, M. Cristofalo, N. Missana, L. Nardo, V. Cassina, A. Tempestini, R. Giovannoni, M. G. Cerrito, N. Zaffroni, T. Bellini, F. Mantegazza, *Biophys. J.* **2016**, *110*, 2151.
- [44] R. Vázquez, S. A. Licandro, L. Astorgues-Xerri, E. Lettera, N. Panini, M. Romano, E. Erba, P. Ubezio, E. Bello, R. Libener, S. Orecchia, F. Grosso, M. E. Riveiro, E. Cvitkovic, M. Bekradda, M. D'Incaldi, R. Frapolli, *Int. J. Cancer* **2017**, *140*, 197.